IAEA
International Atomic Energy Agency

20th IAEA Fusion Energy Conference
Vilamoura, Portugal, 1 to 6 November 2004

IAEA-CN-116/EX/P5-29

FAR SOL TRANSPORT AND MAIN WALL PLASMA INTERACTION IN DIII-D

D.L. RUDAKOV,[1] J.A. BOEDO,[1] R.A. MOYER,[1] P.C. STANGEBY,[2] J.G. WATKINS,[3] D.G. WHYTE,[4] L. ZENG,[5] N.H. BROOKS, R.P. DOERNER,[1] T.E. EVANS, M.E. FENSTERMACHER,[6] M. GROTH,[6] E.M. HOLLMANN,[1] S.I. KRASHENINNIKOV,[1] C.J. LASNIER,[6] A.W. LEONARD, M.A. MAHDAVI, G.R. McKEE,[4] A.G. McLEAN,[2] A.YU. PIGAROV,[1] W.R. WAMPLER,[3] G. WANG,[5] W.P. WEST, and C.P.C. WONG

General Atomics
San Diego, California 92186-5608
United States of America

[1]University of California, San Diego, La Jolla, California 92093-0417, USA
[2]University of Toronto Institute for Aerospace Studies, Toronto, Ontario M3H 5T6, Canada
[3]Sandia National Laboratories, Albuquerque, New Mexico 87185, USA
[4]University of Wisconsin, Madison, Wisconsin 53706, USA
[5]University of California, Los Angeles, California, USA
[6]Lawrence Livermore National Laboratory, Livermore, California 94551, USA

This is a preprint of a paper intended for presentation at a scientific meeting. Because of the provisional nature of its content and since changes of substance or detail may have to be made before publication, the preprint is made available on the understanding that it will not be cited in the literature or in any way be reproduced in its present form. The views expressed and the statements made remain the responsibility of the named author(s); the views do not necessarily reflect those of the government of the designating Member State(s) or of the designating organization(s). In particular, neither the IAEA nor any other organization or body sponsoring this meeting can be held responsible for any material reproduced in this preprint.

Far SOL Transport and Main Wall Plasma Interaction in DIII-D

D.L. Rudakov,[1] J.A. Boedo,[1] R.A. Moyer,[1] P.C. Stangeby,[2] J.G. Watkins,[3] D.G. Whyte,[4] L. Zeng,[5] N.H. Brooks,[6] R.P. Doerner,[1] T.E. Evans,[6] M.E. Fenstermacher,[7] M. Groth,[7] E.M. Hollmann,[1] S.I. Krasheninnikov,[1] C.J. Lasnier,[7] A.W. Leonard,[6] M.A. Mahdavi,[6] G.R. McKee,[4] A.G. McLean,[2] A.Yu. Pigarov,[1] W.R. Wampler,[3] G. Wang,[5] W.P. West,[6] and C.P.C. Wong[6]

[1]University of California, San Diego, La Jolla, California 92093-0417, USA
[2]University of Toronto Institute for Aerospace Studies, Toronto, Ontario M3H 5T6, Canada
[3]Sandia National Laboratories, Albuquerque, New Mexico 87185, USA
[4]University of Wisconsin, Madison, Wisconsin 53706, USA
[5]University of California, Los Angeles, California, USA
[6]General Atomics, P.O. Box 85608, San Diego, California 92186-5608, USA
[7]Lawrence Livermore National Laboratory, Livermore, California 94551, USA

E-mail contact of main author: rudakov@fusion.gat.com

Abstract: Far scrape-off layer (SOL) and near-wall plasma parameters in DIII-D depend strongly on the discharge parameters and confinement regime. In L-mode discharges cross-field transport increases with the average discharge density and flattens far SOL profiles, thus increasing plasma-wall contact. In H-mode between edge localized modes (ELMs), plasma-wall contact is generally weaker than in L-mode. During ELMs plasma fluxes to the wall increase to, or above the L-mode levels. Depending on the discharge conditions ELMs are responsible for 30-90% of the ion flux to the outboard chamber wall. Cross-field fluxes in far SOL are dominated by large amplitude intermittent transport events that may propagate all the way to the outer wall and cause sputtering. A Divertor Material Evaluation System (DiMES) probe containing samples of several ITER-relevant materials including carbon, beryllium and tungsten was exposed to a series of upper single null (USN) discharges as a proxy to measure the first wall erosion.

1. Introducton

Plasma interaction with the main chamber wall is of critical importance for the next-step fusion devices such as ITER. It should be minimized in order to prevent damage to the first wall elements and core plasma contamination with impurities. In most modern tokamaks the isolation of the core plasma from the main chamber wall is accomplished by the use of a poloidal divertor magnetic configuration [1,2], where a magnetic separatrix divides the core plasma from the scrape-off layer (SOL). In an idealized picture of a divertor operation, plasma particles cross the last closed flux surface (LCFS) into the SOL and flow along the open field lines into the divertor volume, where most of the plasma-material interactions (PMI) occur. However, in recent years it has become obvious that this idealized picture does not universally apply. Experiments on Alcator C-Mod [3-5], DIII-D [6-11], ASDEX-Upgrade [12], JET [13,14], and other machines, as well as modeling of the tokamak edge plasmas [3,4,15,16] have shown that under certain conditions plasma contact with the main chamber wall may be significant – even when the distance to the wall is large compared with the density decay length existing at the separatrix. A number of studies have reported fast cross-field convective transport of particles and heat in the tokamak SOL [3-5,7-12,14]. This fast non-diffusive transport, intermittent in time and space, is attributed to coherent structures (also called blobs, streamers, IPOs, filaments, plasmoids, and avaloids) featuring densities and temperatures above those of the background SOL plasma. The intermittent objects (which we will call blobs after Refs. [17-19]) are born in the vicinity of LCFS at the low field side (LFS) of the torus and move towards the wall due to ExB drifts [18,19]. They can propagate ballistically across the SOL, and may reach the main chamber and cause increased PMI levels and impurity production. The intermittent SOL transport is observed under a wide variety of plasma conditions and is the main candidate to explain unexpectedly high levels of the plasma interaction with the main chamber wall in the divertor machines. An alternative viewpoint is that the effect of the fast intermittent transport in the far SOL is to increase the

time-averaged density decay length in that region, significantly above the decay length at the separatrix, thus increasing plasma-wall contact relative to simple expectations.

2. Structure of the DIII-D Low Field Side SOL

Since most of the diagnostics suitable for studies of the SOL transport and evaluation of the plasma fluxes to the main wall are located on the outboard side of the DIII-D chamber, we will concentrate on the LFS SOL. Outer edge and SOL diagnostics in DIII-D include Thomson scattering system, beam emission spectroscopy (BES) system, a fast profile reflectometer, reciprocating probe array, and tangential D_α array.

Figure 1 shows a poloidal cross-section of DIII-D tokamak. Also shown are the LCFS and a few SOL magnetic flux surfaces for a lower single-null (LSN) discharge calculated by EFIT equilibrium fitting code. Immediately adjacent to the LCFS is the near SOL region where the magnetic field lines connect from the outboard to the inboard side of the torus and terminate at the divertor plates or baffles on both ends. We will refer to this region as the "divertor SOL" (DSOL). Radially outwards from the DSOL on the outboard side is a region marked by lighter shading in Fig. 1, where one side of the magnetic field lines terminates on the toroidally symmetric "knee limiter" located at the upper outer side of the vacuum vessel and the other side terminates on the upper surface of the lower divertor baffle structure. This part of the SOL is essentially "limited" by these two surfaces, therefore, we will refer to this region, as "limiter SOL" (LSOL). We should note that the radial width of LSOL depends on the magnetic topology. For some configurations it may totally vanish. Further outwards from the LSOL is the "outer wall shadow" (OWS) region, shown by the darker shaded area in Fig. 1, where the magnetic field lines terminate at the outer wall near the midplane. In this article we regard the two "limiter" surfaces forming the LSOL as main wall elements, thus LSOL and OWS constitute the "wall SOL" (WSOL). We will call the part of the main chamber wall adjacent to the whole WSOL (from Point A to Point B, Fig. 1) "LFS wall", whereas the vertical part (from Point C to Point D) will be referred to as "outer wall" (OW).

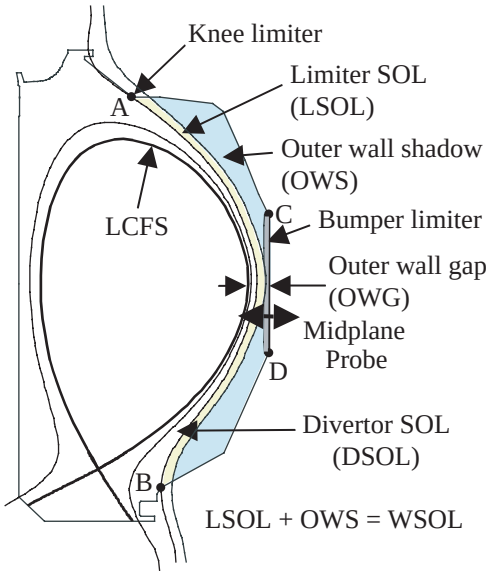

Fig. 1. Diagnostic arrangement and the structure of the DIII-D low field side SOL in a LSN magnetic configuration.

The OWS boundary and the OW are not toroidally symmetric since they feature a large number of diagnostic ports and protruding elements such as bumper limiters and rf antennas. Strictly speaking, the OWS region begins where the magnetic field lines start to terminate at the most protruding elements of the outer wall, the bumper limiters (BLs). In DIII-D there are three of those limiters separated toroidally by approximately 120 degrees and protruding by ~2 cm inwards from the outer wall. However, in the SOL, where the magnetic field lines are open, a toroidally localized object only "casts shadow" over the field lines that are directly connected to it (plus a narrow adjacent area affected via cross-field diffusion). Therefore, we define OWS as the region starting where the magnetic field lines terminate on the OW itself near the midplane. We also define the outer wall gap (OWG) as the minimum distance from the LCFS to the outer wall near the midplane.

3. SOL Profiles, Transport, and Plasma Interaction With the Outer Wall in L-mode

A large set of experimental data was collected over a significant number of low-power L-mode LSN discharges termed simple-as-possible plasmas (SAPP) and aimed at extensive

characterization of the edge and SOL plasma parameters in DIII-D. The typical discharge parameters of SAPP shots were: toroidal magnetic field, B_T = 2 T, plasma current, I_p = 1 MA, average plasma density, $\bar{n}_e$ = 0.25-0.55x10^{19} m^{-3}. Radial profiles (along the probe insertion path) of the SOL plasma density, electron temperature, and normalized density root-mean-square (RMS) fluctuation level, $\tilde{n}_e/n_e$, obtained by the midplane reciprocating probe array for four different average discharge densities are shown in Figs. 2(a-c). The profiles were generated by averaging the probe data over 0.5 ms time intervals and plotting them versus the radial position of the probe [8]. There is generally a reasonably good agreement between the density profiles measured by the probe with those obtained by Thomson scattering and profile reflectometer. The shading in Figs. 2(a-c) corresponds to the convention established in Fig. 1. The radial position of the bumper limiter (mapped along the field onto the probe insertion path) is shown by a gray rectangle. The four density conditions in Fig. 2 correspond to average discharge densities, $\bar{n}_e$, of 2.8, 3.7, 4.3, and 5.3x10^{19} m^{-3} and Greenwald fractions (densities normalized to the Greenwald limit n_{GW} [20]), f_{GW}, of 0.27, 0.35, 0.4 and 0.5, respectively.

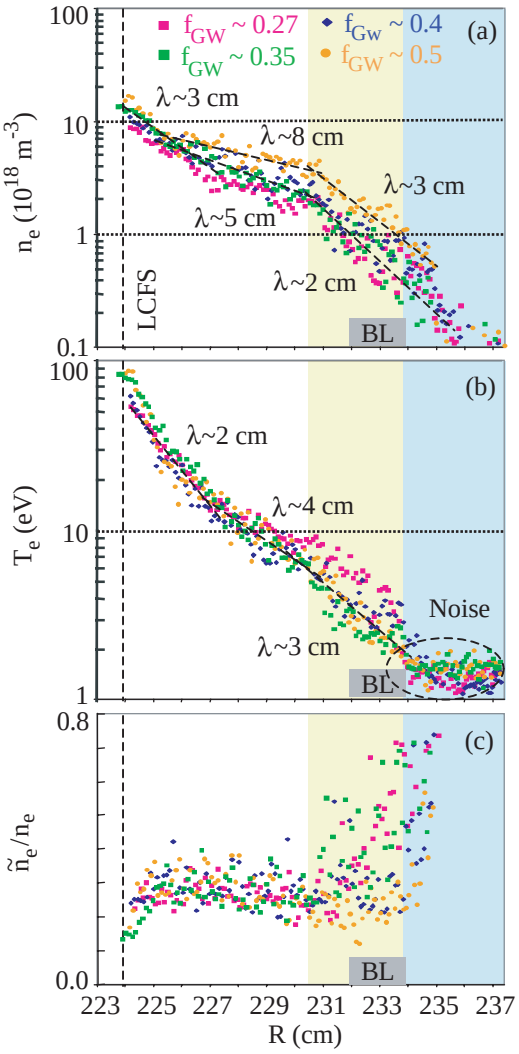

Fig. 2. SOL profiles of the plasma density, electron temperature, and relative density fluctuation level in LSN L-mode discharges with I_p = 1 MA and varying average discharge densities.

The SOL density profiles show three distinct regions: steep exponential decay in the inner part of DSOL just outside the LCFS; flattening (longer decay) in the outer part of DSOL; steeper decay in the LSOL region. The decay lengths of T_e in the DSOL are smaller than those of n_e, while in the LSOL region they are comparable. The bumper limiters have no visible effect on either n_e or T_e profiles (not surprising since none of BLs are connected to the probe along the field lines). As the average discharge density increases, so does the density decay length in the outer part of the DSOL, and the flattening of the density profile in this region becomes more pronounced. The T_e profiles do not change much with the density. Under all conditions time-averaged T_e everywhere in the WSOL is below 10 eV. The relative density fluctuation profiles are flat at about 0.3 through most of the SOL. We should note that the absolute density fluctuation level and the fluctuation-induced cross-field transport in the SOL do increase with the discharge density [7-10].

SOL density profile is largely set by the balance of the perpendicular and parallel transport [21]. Ionization within the SOL affects the density profiles, but the effect is not usually dramatic [21]. In the above examples ionization may be important only in the inner part of the DSOL and not in the WSOL, where T_e is low. The break in the profiles observed at the border between DSOL and LSOL, where a connection length changes in a step-like manner, clearly shows that parallel transport is indeed important in setting the profile shape. The increase of the density decay length in DSOL with $\bar{n}_e$ is a manifestation of the increased ratio of perpendicular to parallel transport. The decay lengths in the LSOL are a factor of 2.5

shorter than those in the DSOL, indicating a stronger effect of parallel transport in the LSOL. Plasma interaction with main chamber is in this case occurring mostly on the surfaces limiting the LSOL that receive most of the fluxes crossing from the DSOL into the WSOL.

If the density decay length in LSOL is smaller than the LSOL width, the magnitude of the total plasma ion flux to the main chamber surfaces limiting LSOL can be readily estimated by applying a "window-frame" analysis technique [21,22]. The estimated ratio of the LFS wall ion flux to the LFS divertor ion flux increases with the discharge density from about 0.1 in attached L-mode to about 0.6 with detachment [22]. This estimate is in reasonable agreement with UEDGE modeling with imposed convection [15,16].

There are situations, however, when significant plasma-wall contact extends through the LSOL to the outer wall. Figure 3(a) presents a comparison of the SOL profiles in the highest density shot from Fig. 2 and a SAPP shot with a slightly lower plasma current, I_p = 0.8 MA. The lower I_p discharge had $\bar{n}_e$ = 4.5x10^{19} m^{-3} and f_{GW} ~ 0.58. The density profiles are remarkably different in the LSOL region where the local densities in the lower I_p case are higher by the factor of 2-3. This indicates that at lower I_p the ratio of perpendicular to parallel transport in LSOL is increased, possibly due to enhanced convection. It is worth noting that an increase of the density scrape-off length at decreased plasma current has been previously observed in the limiter SOL of JET [23].

Previous studies of the fast convective transport by intermittent plasma structures (blobs) in DIII-D have been reported in Refs. [7-11]. The intermittent transport can be a dominant cross-field transport mechanism in the far SOL [8] and is likely to be the key to the difference in the far SOL densities between the two shots in Fig. 3(a). This assumption is substantiated by Fig. 3(b) showing 2 ms portions of the ion saturation current (I_{si}) signals from the outer side of the LSOL (corresponding to R ~ 233 cm) in the two shots from Fig. 3(a). In the lower I_p case, I_{si} features large amplitude (up to 3 times the average level) intermittent events. Enhanced cross-field transport due to these events can explain the higher far SOL densities in the lower I_p case. It has been shown [7-10] that the blobs dissipate particles and heat as they move towards the outer wall. However, the above example demonstrates that in high density discharges the blobs exist deep in the LSOL and can actually reach the outer wall.

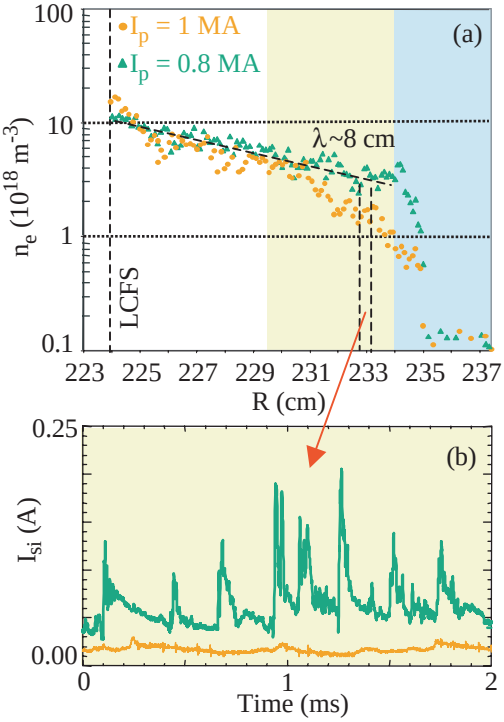

Fig. 3. Comparison of the SOL density profiles in LSN L-mode discharges with I_p = 1 MA and I_p = 0.8 MA (a) and time traces of the ion saturation currents in far SOL (R = 233 cm) of the two discharges (b).

In all the above examples the density profile in the SOL is decaying exponentially in any given region of the SOL, even though the decay lengths are sometimes comparable to the SOL width. Therefore, an increase in the outer wall gap (OWG) is likely to decrease the plasma contact with the LFS wall. This was indeed observed by varying OWG in otherwise similar moderate density (f_{GW} ~ 0.4) SAPP discharges. An increase in OWG by about 2 cm resulted in a decrease of the plasma density at the OWS border by a factor of 3-4 [24].

4. Plasma-Wall Interaction in H-mode and Relative Role of ELMs

Characterization of the SOL profiles and plasma-wall interaction in H-mode is complicated by the presence of Edge Localized Modes (ELMs). SOL plasma parameters and main wall plasma fluxes in-between and during ELMs often differ by more than an order of

magnitude. This is illustrated in Fig. 4, showing the radial profiles of the SOL plasma density (obtained from the midplane probe data in the same way as those in Fig. 2) in a high density L-mode and a moderate density H-mode discharge. The H-mode discharge had a few ELMs that are prominent on the profile. Between the ELMs, density everywhere in the SOL is well below the L-mode level. During ELMs, it increases transiently up to the L-mode level at the corresponding radial position. Therefore, plasma contact with the LFS wall in H-mode is lower between the ELMs and comparable during the ELMs to that in L-mode.

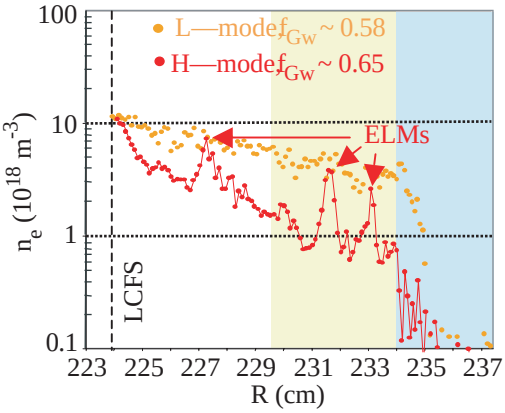

Fig. 4. Comparison of the SOL density profiles in LSN L and H-mode discharges.

Outward expansion of the density profile and transient increase of the SOL plasma density during ELMs was observed by a fast profile reflectometer located at the outer midplane [11, 25]. An example of density profile evolution through a single Type-I ELM in a lower density H-mode discharge (f_{GW} ~ 0.4) is shown in Fig. 5 [25]. The ELM timing is shown by a divertor D_α signal, Fig. 5(a), where the numbers and vertical lines represent the times for the density profile sequence shown in Fig. 1(b). Profile 1, taken just before the ELM onset, shows a typical H-mode steep edge pedestal. At the onset of the ELM, Profile 2 shows an increase in the SOL density, with the density at the top of the pedestal slightly reduced. At the time of the ELM crash, about 100 μs later, Profile 3 has expanded radially outward to the vessel wall, where there is a relatively large density rise of ~2x10^{18} m^{-3}. This profile exhibits no steep pedestal and is reminiscent of an L-mode profile, consistent with the probe data of Fig. 4. During the recovery phase, Profile 4 shows the pedestal gradually rebuilding, and the SOL density reducing. Profile 5 shows a return to a well defined edge pedestal several milliseconds after the ELM onset. Thomson scattering data obtained at the same time as Profile 5 (points with error bars) show good agreement with reflectometer measurements.

The data points in Fig. 4 are averaged over 0.5 ms, a time interval comparable to the ELM duration (of 1-3 ms in this discharge). Transient bursts of the SOL density and temperature observed during ELMs on shorter time scales of tens of microseconds can in fact be of much higher amplitude than the 0.5 ms averages. In the inner part of DSOL n_e and T_e during ELMs increase transiently to the values characteristic of the density pedestal [11,26], indicating that ELMs "peel" from the pedestal. Once separated from the pedestal, ELMs form hot and dense coherent plasma structures propagating radially towards the outer wall. The radial propagation velocity of the ELM density pulse estimated from the reflectometer data, about 500 m/s, is consistent with the ExB velocity measured by the midplane probe array [11].

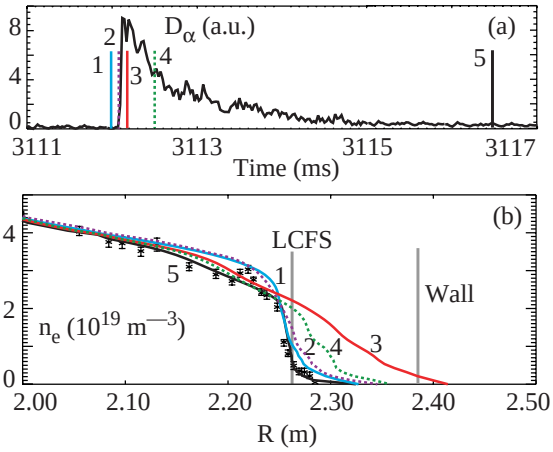

Fig. 5. Density profile evolution during a single ELM.

As the ELM structure propagates towards the wall, it looses particles and heat due to the parallel sink action of the SOL. The energy is lost much faster than particles. The radial decay length of T_e during ELMs, λ_{Te}, is typically about 1.5 cm, while λ_{ne} varies between 3 and 8 cm, depending on the discharge conditions [26]. Therefore ELMs are transporting particles into the WSOL, while most of the ELM heat is lost to the divertor plates.

ELMs observed in the SOL have a complicated spatio-temporal structure [8,11,26]. To the reciprocating probe ELMs in WSOL appear as a sequence of density and temperature bursts closely resembling intermittent events observed in L-mode. This is illustrated in Fig. 6 showing the time series of the plasma density and temperature measured by the midplane probe in WSOL in high density ($\bar{n}_e$ = 6.5x10^{19} m^{-3}, f_{Gw} ~ 0.6) L-mode (a,b), and high density ($\bar{n}_e$ = 1x10^{20} m^{-3}, f_{Gw} ~ 1) H-mode (c,d). The probe is moving, so both time and space scales are shown. Large amplitude intermittent events are obvious in all signals, appearing even in the OWS region in the L-mode case.

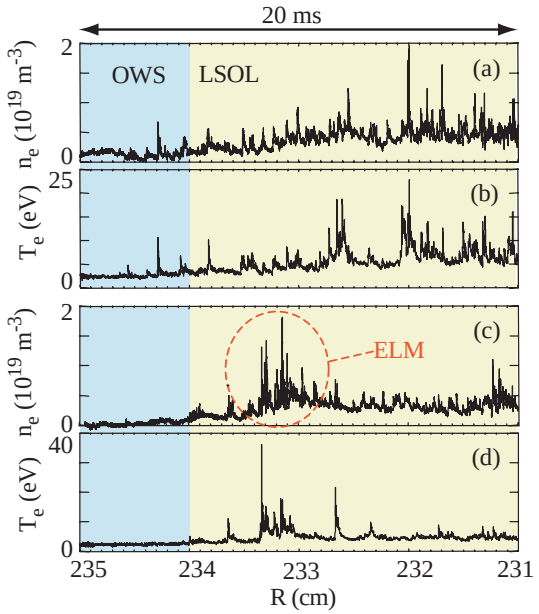

Fig. 6. Time traces (plotted versus the radial position of the probe) of the plasma density and electron temperature in the far SOL of high-density ($\bar{n}_e$ = 6.5x10^{19} m^{-3}, f_{Gw} ~ 0.6) L-mode (a,b) and high density ($\bar{n}_e$ = 1x10^{20} m^{-3}, f_{Gw} ~ 1) H-mode (c,d) discharges.

In some cases ELMs can propagate all the way through the LSOL to the outer wall. Figure 7 shows 100 ms of I_{si} (a) and T_e (b) time series measured by the midplane reciprocating probe fixed in LSOL about 5 mm inwards of the OWS border. During ELMs I_{si} increases transiently up to about 1 A, while the temperature shows only a moderate increase to 15-25 eV. Figure 7(a1-a3) shows 1 ms expanded time frames of the three largest ELMs. We notice that a) all ELMs feature large bursts 15-20 μs in duration followed by lower amplitude "tails", b) some ELMs feature more than one large burst, c) the first burst is not necessarily the largest. We should note that I_{si} ~ 1 A at T_e ~ 20 eV for the probe area used corresponds to the density of about 5x10^{19} m^{-3}, which is the density characteristic of the top of the H-mode pedestal. Therefore, ELMs can bring blobs of very high density to the outer wall.

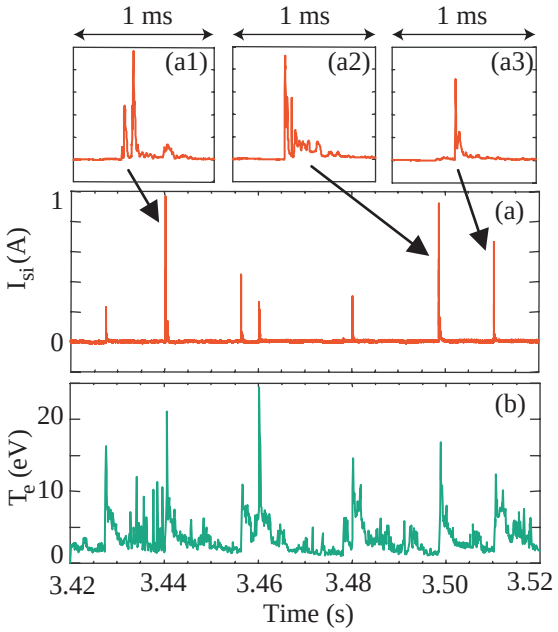

Fig. 7. Time series of (a) I_{si} and (b) T_e measured by the midplane reciprocating probe fixed in LSOL about 5 mm inwards of the OWS border.

A relative contribution of ELMs to the *local* ion wall flux can be estimated from the ion saturation current to the midplane probe in WSOL. If the sheath conditions at the probe are similar to those at the wall, ion flux density collected by the probe should be equal to that at the wall (per projection area perpendicular to the magnetic field). We can then estimate the relative contribution of the ELMs to the total ion wall flux as the ratio of the integral of I_{si} taken during a few ELMs to the total integral of I_{si} over the corresponding time interval including inter-ELM periods:

$$f_{ELM} = \int_{ELM} I_{si} dt \Big/ \int_{total} I_{si} dt \quad . \qquad (1)$$

Depending on the discharge conditions, ELM size and repetition frequency, f_{ELM} varies from about 30% to 90%. Dependence of f_{ELM} in the LSOL on the Greenwald fraction f_{GW} is illustrated in Fig. 8. Though there is no obvious scaling, at the highest densities ($f_{GW} \sim 1$) f_{ELM} tends to decrease due to increased plasma-wall contact between ELMs and reduced ELM amplitude.

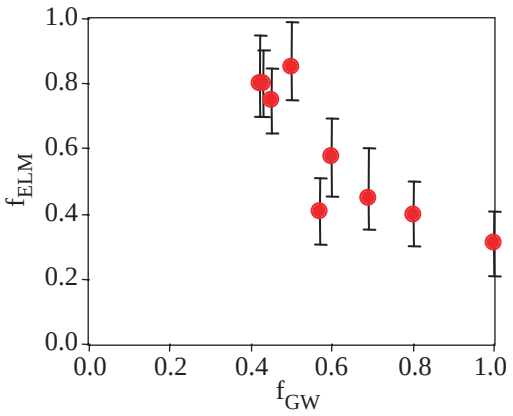

Fig. 8. Dependence of the relative contribution of ELMs to the local ion wall flux near midplane on the normalized discharge density.

5. Main Wall Erosion Studies

DIII-D is equipped with a Divertor Material Evaluation System (DiMES) that allows insertion of material samples into the lower divertor in order to study PMI processes. Plasma conditions in the lower divertor in upper single-null (USN) and inner wall limited (IWL) configurations were found to be comparable to those near the outer wall. Therefore, exposing a sample in the lower divertor in USN or IWL configuration can serve as a good proxy to study the outer wall erosion. A DiMES probe featuring 7 individual samples of ITER-relevant materials including carbon, beryllium and tungsten was exposed to 22 plasma discharges of which 20 were USN and 2 were IWL. All discharges had comparatively low densities. The exposed sample has been analyzed at the Sandia National Laboratories, Albuquerque, by several Ion Beam Analysis (IBA) techniques [27] including Rutherford Backscattering Spectroscopy (RBS) and Nuclear Reaction Analysis (NRA). The measured erosion levels for all materials were near or below the resolution limit of the measurements (of a few nanometers). We are planning to continue the main wall erosion studies with longer exposures and/or higher density conditions to obtain measurable erosion levels. A possibility of creating a capability for exposing material samples on the outboard side of DIII-D chamber is also being discussed.

6. Summary

Direct experimental evidence of main wall plasma contact in DIII-D under a variety of the plasma conditions is observed. In L-mode, cross-field transport increases with the discharge density and elevates the far SOL density, thus increasing plasma-wall interaction. Plasma ion fluxes to the LFS wall increase with decreasing plasma current and with decreasing outer wall gap. In H-mode between ELMs plasma fluxes to the LFS wall are about an order of magnitude lower than those in comparable density L-mode. During ELMs wall fluxes increase to, or above, the L-mode levels. SOL density profiles during ELMs are comparable to those in L-mode. Intermittent density bursts observed in far SOL during ELMs are of similar or larger amplitude than those observed in the same region in L-mode. Depending on the discharge conditions, ELMs are responsible for 30%-90% of the total ion flux at the outboard wall.

Disruptions produce large transient particle and heat loads to the main chamber elements. Discussion of the main wall plasma interaction during disruptions is presented in Ref. [28].

High particle and heat fluxes to the main wall, particularly during ELMs and disruptions, can lead to unacceptable damage to the first wall in the next-step fusion devices. Suitable first wall materials, adequate wall gaps, and operational regimes avoiding large transient loads to the main wall elements have to be used.

Acknowledgments

This work was supported by the U.S. Department of Energy under DE-FG02-04ER54758, DE-FG03-96ER54373, DE-FC02-04ER54698,W-7405-ENG-48, and DE-FG03-01ER54615. Sandia is a multiprogram laboratory operated by Sandia Corporation, a Lockhead Martin Company, for the U.S. Department of Energy under DE-AC04-94AL85000.

References

[1] FENEBERG, W., Phys. Lett. A, **36** (1971) 125.
[2] OHYABU, N., Nucl. Fusion **21** (1981) 5.
[3] UMANSKY, M.V., *et al.,* Phys. Plasmas **5** (1998) 3373.
[4] LaBOMBARD, B., *et al.,* Nucl. Fusion **40** (2000) 2041.
[5] LaBOMBARD, B., *et al.,* Phys. Plasmas **8** (2001) 2107.
[6] WATKINS, J.G., *et al.,* J. Nucl. Mater. **196-198** (1992) 829.
[7] BOEDO, J.A., *et al.,* Phys. Plasmas **8** (2001) 4826.
[8] RUDAKOV, D.L., *et al.,* Plasma Phys. Cont. Fusion **44** (2002), 717.
[9] BOEDO, J.A., *et al.,* J. Nucl. Mater. **313-316** (2003) 813.
[10] BOEDO, J.A., *et al.,* Phys. Plasmas **10** (2003) 1670.
[11] FENSTERMACHER, M.E., *et al.,* Plasma Phys. Control. Fusion **45** (2003) 1597.
[12] KALLENBACH, A., *et al.,* Nucl. Fusion **43** (2003) 573.
[13] GHENDRIH, Ph., *et al.,* J. Nucl. Mater. **313-316** (2003) 914.
[14] GONCLAVES, B., *et al.,* Plasma Phys. Control. Fusion **45** (2003) 1627.
[15] PIGAROV, A.Yu., *et al.,* Phys. Plasmas **9** (2002) 1287.
[16] PIGAROV, A.Yu., *et al.,* J. Nucl. Mater. **313-316** (2003) 1076.
[17] ZWEBEN, S.J., Phys. Fluids **28** (1985) 974.
[18] KRASHENINNIKOV, S.I., Phys. Lett. A **283** (2001) 368.
[19] D'IPPOLITO, D., MYRA, KRASHENINNIKOV, S.I., Phys. Plasmas **9** (2002) 222.
[20] GREENWALD, M., *et al.,* Nucl. Fusion **28** (1988) 2199.
[21] STANGEBY, P.C., Phys. Plasmas **9** (2002) 3489.
[22] WHYTE, D.G., *et al.,* submitted to Plasma Phys. Control. Fusion.
[23] STANGEBY, P.C. and McCRACKEN, G.M., Nucl. Fusion **30,** (1990) 1225.
[24] RUDAKOV, D.L., *et al.,* accepted for publication in J. Nucl. Mater.
[25] ZENG, L., *et al.,* accepted for publication in J. Nucl. Mater.
[26] BOEDO, J.A., *et al.,* accepted for publication in J. Nucl. Mater.
[27] WAMPLER, W.R., *et al.,* J. Nucl. Mater. **233-237** (1996) 791.
[28] HOLLMANN, E.M., *et al.,* this conference.